Local Strain In A 5-Harness Satin Weave Composite Under Static Tension: Part I - Experimental Analysis

S. Daggumati, E. Voet, W. van Paepegem, J. Degrieck, J. Xu, S.V. Lomov, I. Verpoest

Local Strain In A 5-Harness Satin Weave Composite Under Static Tension: Part I - Experimental Analysis

S. Daggumati, E. Voet, W. Van Paepegem, J. Degrieck, J. Xu, S.V. Lomov, I. Verpoest

PII: S0266-3538(11)00140-0
DOI: 10.1016/j.compscitech.2011.03.021
Reference: CSTE 4968

To appear in: *Composites Science and Technology*

Received Date: 9 September 2010
Revised Date: 26 March 2011
Accepted Date: 30 March 2011

Please cite this article as: Daggumati, S., Voet, E., Van Paepegem, W., Degrieck, J., Xu, J., Lomov, S.V., Verpoest, I., Local Strain In A 5-Harness Satin Weave Composite Under Static Tension: Part I - Experimental Analysis, *Composites Science and Technology* (2011), doi: 10.1016/j.compscitech.2011.03.021

LOCAL STRAIN IN A 5-HARNESS SATIN WEAVE COMPOSITE UNDER STATIC TENSION: PART I - EXPERIMENTAL ANALYSIS

S. Daggumati [a*], *E. Voet*[a], *W. Van Paepegem*[a], *J. Degrieck*[a], *J. Xu*[b], *S.V. Lomov*[b], *I. Verpoest*[b]

[a]*Ghent University, Dept. of Materials Science and Engineering, Sint-Pietersnieuwstraat 41, 9000 Gent, Belgium*

[b]*Katholieke Universiteit Leuven, Department of Metallurgy and Materials Engineering, Kasteelpark Arenberg 44, B-3001 Leuven, Belgium*

ABSTRACT

This paper presents an experimental method for determining the local strain distribution in the plies of a thermoplastic 5-harness satin weave composite under uni-axial static tensile load. In contrast to unidirectional composites, the yarn interlacing pattern in textile composites causes heterogeneous strain fields with large strain gradients around the yarn crimp regions. In addition, depending on the local constraints that are imposed by the surrounding plies, the deformation behaviour of the laminate inner layers may vary from that of the surface layers, which are relatively more free to deform, compared to the inner layers. In order to validate the above hypothesis, the local strains on the composite surface were measured using digital image correlation technique (LIMESS). Internal strains in the composite laminate were measured using embedded Fibre Optic Sensors (FOS).

---

*Corresponding author. Tel.: +32 92 64 33 17; fax: +32 92 64 35 87.
E-mail address: Subbareddy.Daggumati@ugent.be

Based on the DIC results, the strain profiles at various locations on the composite surface were estimated. Using the FOS results, the maximum and minimum strain values in the laminate inner layers were evaluated. Comparison of the local strain values at different laminate positions provides an estimate of the influence of the adjacent layers on the local longitudinal strain behaviour of a satin weave composite. Part II of this paper elucidates the local strain variation computed using the meso-FE simulations. In addition to the comparison of numerical and experimental strain profiles, Part II presents the maximum and minimum strain envelopes for the carbon-PPS (PolyPhenelyne Sulphide) thermoplastic 5-harness satin weave composite.

Keywords: A. Textile composite; B. Local strain analysis; D. Fibre Bragg gratings; D. Digital image correlation

1. Introduction

In order to understand the complex structural deformation behaviour of a textile reinforced composite, local strain analysis is a valuable technique. Due to the heterogeneity of textile composites, classical electrical resistance strain gauges do not have adequate spatial resolution and only a full-field strain measuring technique with high spatial resolution and strain sensitivity can be applied to determine local strain profiles [1]. The local strain measurements obtained from the full-field method will provide a qualitative (spatial strain distribution) as well as quantitative (strain values) understanding of the maximum and minimum values of local strains, and their corresponding locations on the laminate traction free surface.

However, there are few publications [2-4] that have studied the effect of adjacent layers in the textile laminate on the local strain behaviour. The studies mentioned above suggest that the surface strain field is a representative strain field for all layers, which may not be a reliable assumption. As adjacent layers try to suppress the yarn undulation effects of the laminate inner layers, they cause the local strain profile / gradient inside the laminate to vary considerably compared to the surface layers [5, 6]. Moreover, it is important to understand the maximum and minimum strain locations due to the fact that these locations indicate the probable damage initiation zones in a textile laminate [2, 7, 8].

Based on the above discussion, in order to quantify the local strains on the surface layers as well as inside the laminate, the following experimental approach is employed during the tensile test of the composite specimen: a) the local strain on the composite surface is quantified using the digital image correlation technique (LIMESS [9]) together with surface mounted fibre optic sensors (FBG-Fibre Bragg Grating); b) embedded fibre optic sensors were used to obtain the maximum and minimum local strain values inside the laminate. The motivation for the use of this experimental procedure is obtained from the work of [10, 11].

Using the above mentioned experimental techniques, the local strain spatial distribution and the corresponding strain values are evaluated on the composite surface using full-field strain measurements. Moreover, surface mounted FBGs provided the quantitative local strain values. Comparison of the local strain values on the composite surface obtained from the two independent experimental techniques proves the accuracy of the obtained local strain values. Finally, damage initiation on the composite surface is detected using the LIMESS strain data.

For the quantification of local strains inside the laminate, the only possible experimental technique of fibre optic sensors is employed. Based on the comparison of the local strain values at different locations that were obtained using various experimental techniques, an attempt was made to understand the "shadowing" effects on the local strain behavior caused by the interaction of randomly placed plies. Moreover, the large amount of available experimental data helps in the development of an accurate unit cell computational model for evaluating the local strain profiles using meso-FE simulations, which is the subject of Part II of this paper series.

2. Materials and Methods

2.1. Material

The material under study is a thermoplastic 5-harness satin weave composite (CD0286 supplied by 'TenCate'), which has T300 JB carbon fibres as a reinforcement and PPS (PolyPhenylene Sulphide) as a matrix. The composite laminate is manufactured using the compression moulding technique, and has eight layers of satin weave fabric with 50:50 weight ratio in the warp and weft directions. The details of the 5-harness satin weave fabric are listed in Table 1. Composite samples used for the tensile tests were prepared according to the ASTM D3479 standard (width 25 mm, gauge length 170 mm, thickness 2.5 mm) with the end tabs of the same material (Carbon-PPS). Tensile tests were conducted on a standard Instron machine (cross head speed 1mm / min) in a displacement controlled manner.

2.2. Experimental methods

2.2.1. Surface strain measurement (full-field strain measuring technique - DIC)

Digital Image Correlation (DIC) is a non-contact method for measuring the whole-field displacements in 2D and 3D. In addition, DIC is able to capture severe strain gradients at a close location, thus indicating high spatial resolution [12].

The working principle of DIC as well as the theoretical background for the calculation of strains has been explained by many researchers [12-14]. In order to capture the surface strain field during the tensile test, an approximate length of 40 mm ($\cong 5$ unit cells) in the tensile direction and 25 mm ($\cong 3$ unit cells) in the transverse / width direction is painted with a white spray followed by a black speckle pattern on the surface of the white paint at the centre of the composite specimen (Figure 1). For the full-field strain registration during the loading process, the CCD camera was set to capture 2 images / sec over the entire speckle pattern ($40 \times 25\,\text{mm}^2$) (Figure 1). The details of the LIMESS equipment used for full-field strain registration are shown in Table 2. Using the correlation between the initial image of the virgin specimen recorded before any loading and the consequent images taken until just before the final failure of the composite specimen (1.19% of average tensile strain), the local strains were computed at different locations on the laminate surface using the 'Vic 2D' [5] software. The average strain is computed across the entire window of the speckle pattern used for full-field strain registration (Figure 1).

2.2.2. *Local strain measurement using FBGs*

Fibre optic sensors with fibre Bragg gratings (FBGs) are commonly used for local strain sensing, which makes them the optical counterpart to electrical strain gauges. An FBG is a sensitive element written in the core of an optical fibre. The refractive index changes periodically along a definite length in the fibre, acting as a reflector for a specific wavelength (Figure 2).

The reflection spectrum is centred around the Bragg-wavelength λ_B which is given by the condition $\lambda_B = 2n_{eff}\Lambda_{FBG}$, in which n_{eff} is the effective refractive index of the core of the optical fibre and Λ_{FBG} is the period of the grating. An FBG has typical dimensions of a few millimeters in length and a diameter of about 0.2 mm. In this study, high strength coated FBGs i.e. DTG®s (Draw Tower Gratings) were used. They can withstand high strain levels and have been found to be suitable for embedding in thermoplastic composites [15, 16].

The approach employed with regard to the use of fibre optic sensors in the current study is twofold: 1) FBGs were being mounted on the surface of the test specimens to measure local surface strains (Figure 3 left); 2) in order to capture the interior strains around the sensors, FBGs were directly embedded between layers of satin weave fabric during the composite manufacturing process (Figures 3 right). In both approaches we have used sensors with a length of 8 mm (covering the complete length of one unit cell, i.e. 7.4 mm). All the sensors were connected to a commercial Bragg interrogator from FOS&S (FBG-SCAN 608) with a depolarized optical source. Both the Bragg interrogator and the test bench were linked to a PC and all read-out parameters (force, strain, Bragg spectra) were integrated in one software. During stepwise loading (quasi-static testing) of the samples we were able to capture the spectra at each load step. The full spectral response of the FBG sensors and thus the complete Bragg peak deformation was examined for strain analysis.

A varying or non-uniform strain field (e.g. chirped strain field) along a uniform fibre Bragg grating is in fact causing the reflected Bragg peak to split into multiple Bragg peaks. A varying strain distribution will produce a complicated reflected spectrum, however, this effect has been elaborated already by several researchers and is described in literature for transverse and longitudinal applied strains [17-19].

In general, the experimental spectral response to non-uniform strain fields is validated using simulated Bragg spectra where the grating is considered as an initially non-uniform grating subjected to a uniform strain field [17, 18], or to simulate the response of the Bragg grating to damage effects and different crack lengths [19]. The aforementioned procedure confirms that we can determine and simulate complex local (microscopic) strain distributions along the length of the grating from the full distorted Bragg spectrum and that the peak-splitting is related to minimum and maximum (peak) wavelength shifts. Botsis et al. [20] used a more sophisticated method to examine non-uniform strains along gratings from complex reflection spectra. In [20] the spectral response and local Bragg wavelength evolutions are examined for an FBG partially embedded in cylindrical epoxy specimens. An Optical Low Coherence Reflectometry (OLCR)-based technique [21] is used to interrogate the FBG to obtain measurements of the local Bragg wavelength distribution due to non-uniform strain effects. The OLCR based technique allows linking the spatial strain distribution with spectral response. However, this technique is not applied in the work presented here.

Hence the authors are not able to directly relate the minimum and maximum peaks (and peak shifts) to the local spatial distribution along the grating structure. In this work the authors used the digital image correlation (DIC) and meso-FE simulations to validate the minimum and maximum strain readings determined from the distorted peaks. Peak distortion induced by the local non-uniform strain along the grating resulted in multiple small Bragg peaks (Figure 4). By converting the individual Bragg peak shifts into strain with respect to the initial Bragg peak it is possible to calculate the local longitudinal maximum and minimum strain values along the grating length (8 mm) at specific loading levels.

2.2.2. a. Surface local strain field measurement using FBGs

Three test coupons were prepared with each specimen having two surface bonded 80 µm DTG® (high strength FBGs) sensors positioned in the central axis along the load carrying warp yarns. The 80 µm diameter sensors have a total diameter with ORMOCER® coating of approximately 140 µm and an FBG length of 8 mm. A special method of the company FOS&S has been employed to fix the surface sensors in a controlled manner using a UV adhesive and a special sensor pad (patent WO2009106576 (A1)) (Figure 3 (left)). With regard to the specimen preparation, the used methodology is similar to the fixation of electrical strain gauges to the composite specimen. Grinding paper and alcohol are used to prepare the specimen and degrease the specimen and sensor.

In order to position the optical fibre, a fixation method is applied based on UV-curable glue and a UV transparent sensor pad. First, the UV curable glue is spread along the sensor zone (approximately 30 mm x 8 mm) and the fibre with FBG is positioned manually using the UV transparent sensor pad. Later, the optical fibre is gently pushed against the composite specimen using a glass plate on top of the sensor pad and in the same time a first UV pre-cure is applied by illuminating the location of the sensor zone through the UV transparent pad for approximately 30 seconds. After the pre-cure, the glue has become stiff, and the sensor pad can be removed to apply a post-cure by illuminating the sensor zone for approximately 5 minutes. The FBG sensor is now fixed to the specimen and ready to be utilized for local strain measurements.

2.2.2b. Embedded local strain field measurements using FBGs

In addition to the surface bonded sensors, the three test coupons mentioned above contain an embedded 125 µm DTG® sensor placed in the central plane between two woven fabrics (Figure 3 right). The 125 µm diameter sensors have a total diameter with ORMOCER® coating of approximately 190 µm and an FBG length of 8 mm. In order to measure the maximum and minimum strain values of the satin weave composite, the length of the DTG is selected in such a way that it is little longer than the length of a satin weave unit cell (7.4 mm). It should be emphasized that the embedded sensor is surrounded by matrix material, yarns and warp and weft yarn cross-over points inducing a more complex strain field compared to the surface mounted sensors.

It is therefore important to distinguish the transversal effects on the longitudinal strain measuring capabilities of the optical fibres. Previous research of Voet et al. [22] has shown that transversal strains cause: i) optical birefringence effects in the core of the optical fibre; ii) non-uniform strain along the length of the FBG causing an in-fibre strain distribution. Both effects can be characterized by looking into the reflected spectrum of the Bragg peak. In addition, there is a strong correlation between the strain field acting on the embedded grating and the deformation of the reflected Bragg spectrum [18, 23]. However, further investigations on this issue have shown that the birefringence effect in the thermoplastic test specimens is mainly caused by the residual transverse stresses induced during the manufacturing process of the composite, and does not change significantly during the load process; i.e. from the beginning to the end of the loading process this effect stays more or less the same (below strain levels of 0.05%). It can be stated that the Bragg peak deformations examined in this study were principally induced by longitudinal strain effects along the Bragg grating.

Finally, cross-sectional view of the composite laminate with an embedded optical fibre (Figure 5a & b) after the final failure of the composite showed that the optical fibre remained completely bonded to the host composite material, which ensured the correct and constant measuring of the local strains.

3. Results and discussion

Initially, the DIC data is used for the local strain analysis followed by damage detection on the composite surface. Figure 6(a & b) shows the typical longitudinal local surface strain pattern of the satin weave composite under uni-axial tensile load at 0.5% and 1.19% of average tensile strain in the warp yarn direction. Based on the surface strain contours (Figure 6b), it is evident that the maximum strain concentration occurs in a periodic manner at an angle of 26.6^{o} from the perpendicular weft yarn at the yarn crimp location. The angle at which the maximum tensile strain is detected belongs to the weft yarns at the yarn cross-over positions, caused by the weaving pattern of the 5-harness satin weave composite (Figure 6b). Figure 6c shows the typical longitudinal (x-direction) local strain profiles and their evolution on the composite surface at 0.5% and 1.19% of the average tensile strains respectively. By plotting the longitudinal local strain profile at various locations on the composite surface over the length of one unit cell (7.4 mm) starting from one yarn crimp location to another in the load direction (marked locations in Figure 6a), the maximum local strain of 1.49% is observed at the centre of the weft yarn at the yarn crimp location for the applied 1.19% average strain. The entire local longitudinal strain distribution on the composite surface (Figure 6c) can be categorized into three major parts:

- Maximum local longitudinal strain (1.3-1.49%) on the composite surface occurred at the centre of the weft yarn at the yarn crimp locations.

- Minimum local longitudinal strain (1.0-1.15%) in the entire surface strain field is observed in the matrix (resin) pockets at the geometrical transition location between the load carrying warp yarn and the perpendicular weft yarn as marked in Figure 6c.
- Finally, the third phase of the local longitudinal strain is detected at the straight portion of the load carrying warp yarn, which varies (1.15-1.25%) in the close limits of the applied average tensile strain to the composite.

Based on the local strain variation as well as the spatial strain distribution observed from the DIC measurements, the strain gradient is computed as explained in [24]. From the maximum strain location at the centre of the weft yarn to the adjacent matrix pocket (minimum strain) over the length of 1.22 mm, the maximum strain gradient of $3.9\times10^{-3}\,mm^{-1}$ is observed in the marked location 1-2 (Figure 6c).

From the transverse strain pattern (Figure 7a), it is observed that the maximum and minimum transverse strain occurs in a periodic manner at an angle of 63.4^{0} to the perpendicular weft yarn. As marked in Figure 7a, the transverse strain profiles are plotted between the two yarn crimp locations in the y-direction at different locations on the composite surface. From Figure 7b it is observed that the initial phase of the transverse strain profile starts from the centre of the weft yarn at the yarn crimp location with the slight positive transverse strain.

The second and the third phase of the strain profile undergoes the compressive strain at the resin pockets as well as at the straight portion of the load carrying warp yarn. The maximum compressive strain of around 0.027% is detected at the warp yarn. Finally, the maximum in-plane shear strain is detected in the matrix pockets in between the four adjacent yarns.

Apart from the local strain analysis, the DIC results were also used for the detection of local damage (weft yarn cracking) on the composite surface. According to Summerscale et al. [7], by the application of the uni-axial tensile load to the warp yarns, fibres experiencing the highest tension (warp) are straightened more than those under lower strain (weft). As a consequence, the fibres at the non-contact edge of the weft yarn at the yarn crimp location take a longer path than those at the point of contact, thus indicating the possible damage initiation location. The damage initiation at the highest curved point, i.e. the weft yarn at the yarn crimp is detected using the LIMESS local strain data. In order to detect the weft yarn damage, two different procedures can be found in the literature [8, 25], both using almost the same principle. According to [25, 26] at a certain value of the average tensile strain, the local strain E_{xx} at a particular chosen point jumps abruptly, indicating the crack initiation.

Based on the above theory, the local strain is plotted as a function of the applied average strain at different locations of the surface weft yarns at the yarn crimp location. From Figure 8b, at the average tensile strain of around 0.7%, the jump in local strain is detected on the surface weft yarns indicating the damage initiation. The damage locations are marked in Figure 8a. As shown in Figure 8b, once the damage initiation occurred, the linear relationship between the local and global strain is disturbed. In addition, it is observed that the occurrence of damage on the laminate surface is not periodic, which is indicated by the localization of the strain concentration at random locations on the surface weft yarns (Figure 8a). In correlation with the damage initiation obtained from the DIC, microscopic analysis on the polished edges of the tensile tested composite laminate shows that the weft yarn crack occurred at around 0.6-0.8% of the average tensile strain [27] (Figure 8c).

In order to compare the DIC local strain data with the FBG local strains, the following approach is employed. Based on experimental acoustic emission and microscopic analysis of the same composite material, it has been already shown by the authors [27, 28] that the damage initiation in different layers of the satin weave composite is a sequential process. Damage initiation began in the laminate inner layers at 0.2%, followed by damage initiation on the surface layers at around 0.6% of the average tensile strain. In order to avoid the complexities posed by the damage initiation and propagation on the strain measuring capabilities of the optical fibre, the comparison of local strain between the DIC and FBG is accomplished in the elastic range.

Comparison of the local strain values obtained from the DIC and the FBG on the composite surface is accomplished at the average tensile strain of $0.5 \pm 0.01\,\%$ in the load carrying warp direction, and shows very good correlation (Table 3). In addition, the local strain values measured using FBG sensors at different locations of the laminate show that the maximum and minimum local strain values in the laminate inner layers is almost equal to the surface local strains at the same applied average strain. Moreover, in the composite inner layers the local strain values were registered in the elastic range till 0.2% global tensile strain. The maximum and minimum local strains were approximately 0.25 and 0.16% respectively. Later these strains will be compared to the FE simulations (Part II).

4. CONCLUSIONS

Comprehensive local strain analysis is performed on a thermoplastic carbon-PPS 5-harness satin weave composite under uni-axial static tensile load. For the analysis of local strain on the laminate surface, full-field strain measuring technique (DIC) is applied along with fibre optic sensors. In order to detect the local strain inside the laminate, fibre optic sensors were embedded into the laminate during the manufacturing process of the composite. Analysis of the experimental local strain data has lead to the following conclusions:

- The maximum local longitudinal strain on the laminate surface occurs at the centre of the weft yarn at the yarn crimp location, while the minimum strain occurs in the resin pockets adjacent to the yarn crimp locations. In addition, the maximum local longitudinal strain and damage initiation is detected at the same location, i.e. the centre of the weft yarn at the yarn crimp location.
- Along the straight portion of the warp yarn, the local longitudinal strain is almost equal to the average tensile strain applied to the laminate.
- At the applied average tensile strain of 0.5%, the local maximum and minimum strain values obtained from the surface mounted and embedded optical fibres show almost the same strain, indicating that the effects of 'shadowing' are negligible on the local longitudinal strain behavior in the plies of a satin weave composite.
- The surface strain spatial distribution observed in the current study is compared to the maximum and minimum strain locations that have been observed in other studies on plain and twill weave composites [4, 29] under uni-axial static tensile load, using the digital phase shifting grating shearography technique. From the above observations, it might be concluded that for all 2D woven composites, the local in-plane strain components, such as longitudinal, transverse, shear strain behavior is similar on the composite traction free surface in the width direction.

Finally, consistency in the local strain values obtained from the different experimental techniques demonstrates the accuracy of the used experimental procedures. Part II of this paper presents the meso-FE analysis of the local strain using unit cell FE analysis as well as a comparison of the experimental and numerical strains.

ACKNOWLEDGEMENTS

The authors would like to acknowledge the FWO-Vlaanderen for the financial support provided through the project G.0233.06H. The assistance provided by the laboratory staff, Kris van der Staey and Johan Vanhuist, at the department of MTM is gratefully acknowledged. The authors also express their gratitude to 'TenCate Advanced Composites (The Netherlands)' for supplying the composite plates.

REFERENCES

[1] Nicoletto, G., G. Anzelotti, and E. Riva, *Mesoscopic strain fields in woven composites: Experiments vs. finite element modeling.* Optics and Lasers in Engineering. **47**(3-4): p. 352-359.

[2] Potluri, P., Young, R. J., Rashed, K., Manan, A. *Meso-scale strain mapping in UD woven composites.* Composites Part A: Applied Science and Manufacturing, 2009. **40**(12): p. 1838-1845.

[3] Lee, J.-R., Molimard, J., Vautrin, A, and Surrel, Y. *Digital phase-shifting grating shearography for experimental analysis of fabric composites under tension.* Composites Part A: Applied Science and Manufacturing, 2004. **35**(7-8): p. 849-859.

[4] Lomov, S.V., Ivanov, D S., Verpoest, I., Zako, M., Kurashiki, T., Nakai, H., Molimard, J., Vautrin, A. *Full-field strain measurements for validation of meso-FE analysis of textile composites.* Composites Part A: Applied Science and Manufacturing, 2008. **39**(8): p. 1218-1231.

[5] Ivanov, D S., Ivanov, S., Lomov, S, and Verpoest, I. *Strain mapping analysis of textile composites.* Optics and Lasers in Engineering. **47**(3-4): p. 360-370.

[6] Ivanov, D.S. *Damage analysis in textile composites.* PhD Thesis; KU Leuven - Faculty of Engineering, May 2009.

[7] Summerscales, J. and P.M. Russel, *Observations on the fibre distribution and fibre strain in a woven fabric reinforcement.* Advanced composite letters 2004. **23 No.3, 2004**.

[8] Littell, J.D. and W.K. Binienda, *Characterization of Damage in Triaxial Braid Composites Under Tensile Loading.* NASA/TM—2009-215645, May 2009.

[9] Colin de Verdiere, M., Pickett, A. K., Skordos, A. A., Witzel, V. *Evaluation of the mechanical and damage behaviour of tufted non crimped fabric composites using full field measurements.* Composites Science and Technology, 2009. **69**(2): p. 131-138.

[10] Bosia, F., Botsis, J., Facchini, M., Giaccari, P. *Deformation characteristics of composite laminates--part I: speckle interferometry and embedded Bragg grating sensor measurements.* Composites Science and Technology, 2002. **62**(1): p. 41-54.

[11] Bosia, F., T. Gmür, and J. Botsis. *Deformation characteristics of composite laminates--part II: an experimental/numerical study on equivalent single-layer theories.* Composites Science and Technology, 2002. **62**(1): p. 55-66.

[12] Anzelotti, G., G. Nicoletto, and E. Riva, *Mesomechanic strain analysis of twill-weave composite lamina under unidirectional in-plane tension.* Composites Part A: Applied Science and Manufacturing, 2008. **39**(8): p. 1294-1301.

[13] Takano, N., Zako, M., Fujitsu, R., Nishiyabu, K. *Study on large deformation characteristics of knitted fabric reinforced thermoplastic composites at forming temperature by digital image-based strain measurement technique.* Composites Science and Technology, 2004. **64**(13-14): p. 2153-2163.

[14] Grédiac, M., *The use of full-field measurement methods in composite material characterization: interest and limitations.* Composites Part A: Applied Science and Manufacturing, 2004. **35**(7-8): p. 751-761.

[15] Ives, D.B., *Strain Monitoring in Thermoplastic Composites with Optical Fiber Sensors: Embedding Process, Visualization with Micro-tomography, and Fatigue Results.* Journal of Thermoplastic Composite Materials, 2007.

[16] Parlevliet, P.P., *Residual Strains in Thick Thermoplastic Composites - an Experimental Approach.* PhD Thesis; Delft University of Technology, 2010.

[17] Peters, K., Studer, M., Botsis, J., Iocco, A., Limberger, H., Salathé, R. *Embedded optical fiber Bragg grating sensor in a nonuniform strain field: Measurements and simulations.* Experimental Mechanics, 2001. **41**(1): p. 19-28.

[18] Ling, H.-Y., Lau, K-T., Jin, W., Chan, K-C. *Characterization of dynamic strain measurement using reflection spectrum from a fiber Bragg grating.* Optics Communications, 2007. **270**(1): p. 25-30.

[19] Prabhugoud, M. and K. Peters, *Efficient simulation of Bragg grating sensors for implementation to damage identification in composites.* Smart Materials and Structures, 2003. **12**(6): p. 914.

[20] Karalekas, D., J. Cugnoni, and J. Botsis, *Monitoring of process induced strains in a single fibre composite using FBG sensor: A methodological study.* Composites Part A: Applied Science and Manufacturing, 2008. **39**(7): p. 1118-1127.

[21] Giaccari, P. and et al., *On a direct determination of non-uniform internal strain fields using fibre Bragg gratings.* Smart Materials and Structures, 2005. **14**(1): p. 127.

[22] Voet, E. and et al., *High strain measurements during fatigue cycleing in fibre reinforced thermoplastic composites using imbedded draw tower fibre brag grating sensors* ECCM13 Conference procedings, 2008.

[23] YipingWang, Binfeng Y., Na C., Yiping C. *Characterization of a high birefringence fibre Bragg grating sensor subjected to non-homogeneous transverse strain fields.* Meas. Sci. Technol. 17 939-942 2006.

[24] Lagattu, F., J. Brillaud, and M.-C. Lafarie-Frenot, *High strain gradient measurements by using digital image correlation technique.* Materials Characterization, 2004. **53**(1): p. 17-28.

[25] Ivanov, D.S., Bogdanovich, A.E., Lomov, S.V., Mungalov, D., Karahan, M., Verpoest, I. *A comparative study of tensile properties of non-crimp 3D orthogonal weave and multi-layer plain weave E-glass composites. Part 2: Comprehensive experimental results.* Composites Part A: Applied Science and Manufacturing, 2009. **40**(8): p. 1144-1157.

[26] Koissin, V., Kustermans, J., Lomov, S. V., Verpoest, I., Van Den Broucke, B., Witzel, V. *Structurally stitched NCF preforms: Quasi-static response.* Composites Science and Technology, 2009. **69**(15-16): p. 2701-2710.

[27] Daggumati, S., De Baere, I., Van Paepegem, W., Degrieck, J., Xu, J., Lomov, S. V., Verpoest, I. *Local damage in a 5-harness satin weave composite under static tension: Part I - Experimental analysis.* Composites Science and Technology. **70**(13): p. 1926-1933.

[28] Daggumati, S., Van Paepegem, W., Degrieck, J., Xu, J., Lomov, S. V., Verpoest, I. *Local damage in a 5-harness satin weave composite under static tension: Part II - Meso-FE modelling.* Composites Science and Technology. **70**(13): p. 1934-1941.

[29] Lee, J.-R., Molimard, J., Vautrin, A., Surrel, Y. *Diffraction grating interferometers for mechanical characterisations of advanced fabric laminates.* Optics & Laser Technology, 2006. **38**(1): p. 51-66.

[30] Lomov, S.V., Ivanov, D.S., Bogdanovich, A.E., Mungalov, D., Karahan, M., Verpoest, I. *A comparative study of tensile properties of non-crimp 3D orthogonal weave and multi-layer plain weave E-glass composites. Part 1: Materials, methods and principal results.* Composites Part A: Applied Science and Manufacturing, 2009. **40**(8): p. 1134-1143.

Table 1. 5-harness satin weave carbon-PPS composite information.

Carbon fibre type	*T300JB*
Linear density TEX, (g/km)	*198*
End/Pick count, yarns per10 cm	*70*
Yarn filament count	*3000*
Filament diameter, (mm)	*0.007*
Carbon fibre density, (g/cm^3)	*1.75*
Fabric areal density, (g/m^2)	*285*
Number of layers	*8*
Overall fibre volume fraction	*50± 3%*
Laminate thickness, mm	*2.5*

Table 2. Details of the strain mapping (LIMESS) equipment [30].

Software	*LIMESS – Vic 2D*
Camera	*12 bit grayscale 1392×1040 pix*
Lens focus distance, mm	*16*
Correlation subset size, pixels	*21*
Correlation step size, pixels	*5*
Strain window, pixels	*5*
Accuracy for strain, μ strains	*200 (=0.02%)*

Table 3. Comparison of the local longitudinal strain values - DIC vs. FBGs.

	Average strain	*Local strain at the yarn crimp(weft), %*	*Local strain at the flat yarn (warp),%*	*Local strain in the matrix,%*
FBGs –inside	(0.2 ± 0.01) %	*0.25*	*-NA-*	*0.16*
FBGs –inside	(0.5 ± 0.01) %	*0.55-0.57*	*-NA-*	*0.43-0.45*
FBGs -surface	(0.5 ± 0.01) %	*0.56-0.57*	*-NA-*	*0.42-0.45*
DIC	(0.5 ± 0.01) %	*0.58-0.62*	*0.48-0.52*	*0.43-0.46*

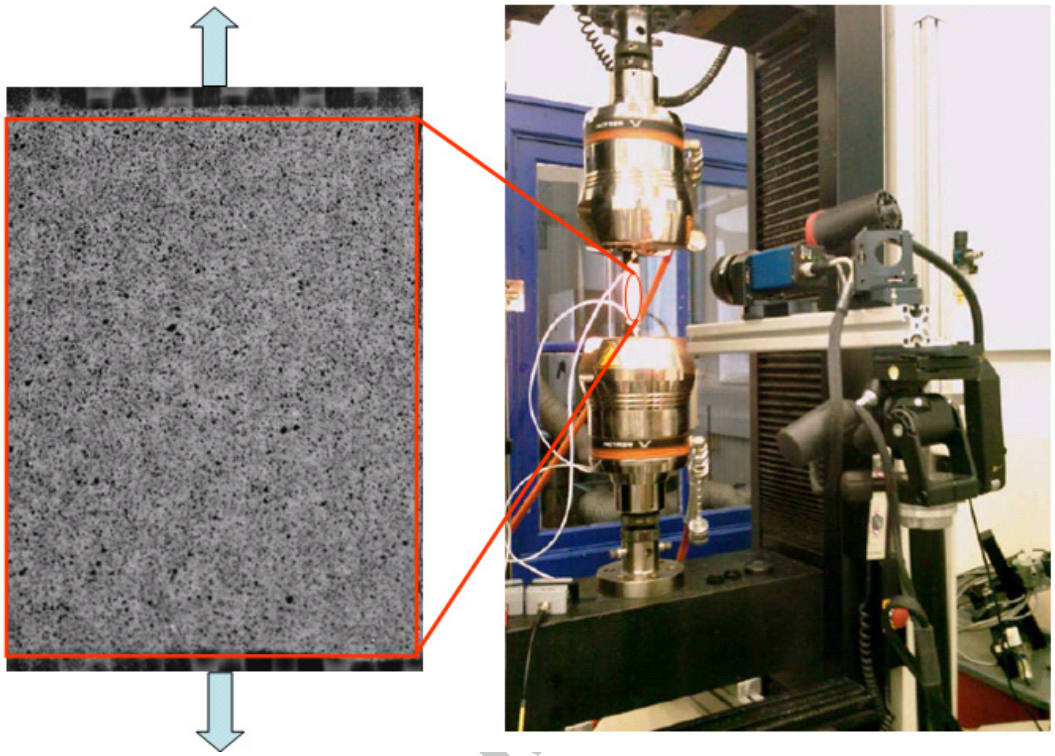

Figure 1. **Specimen with DIC pattern and experimental setup.**

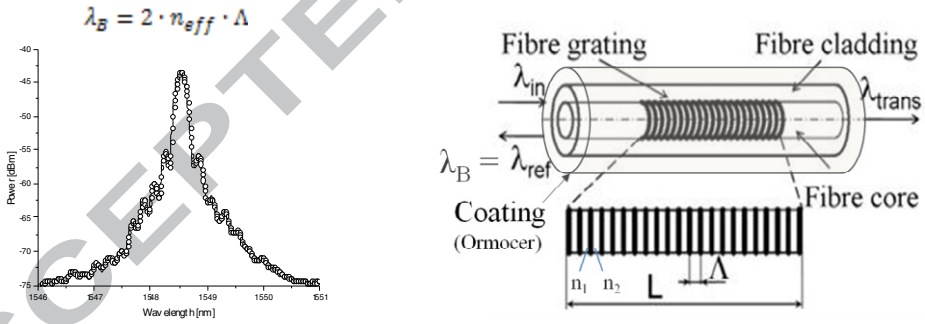

Figure 2. **Typical reflected Bragg spectrum and FBG sensor in the fibre core.**

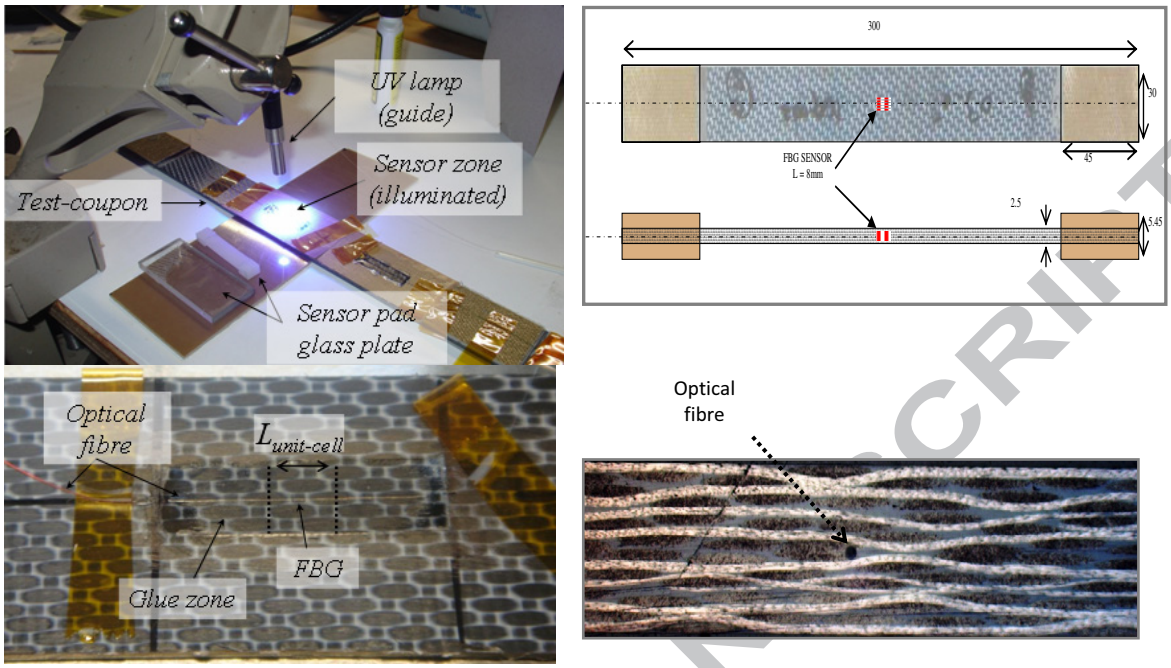

Figure 3. **Surface mounting (left), embedded FBG with cross sectional view (right).**

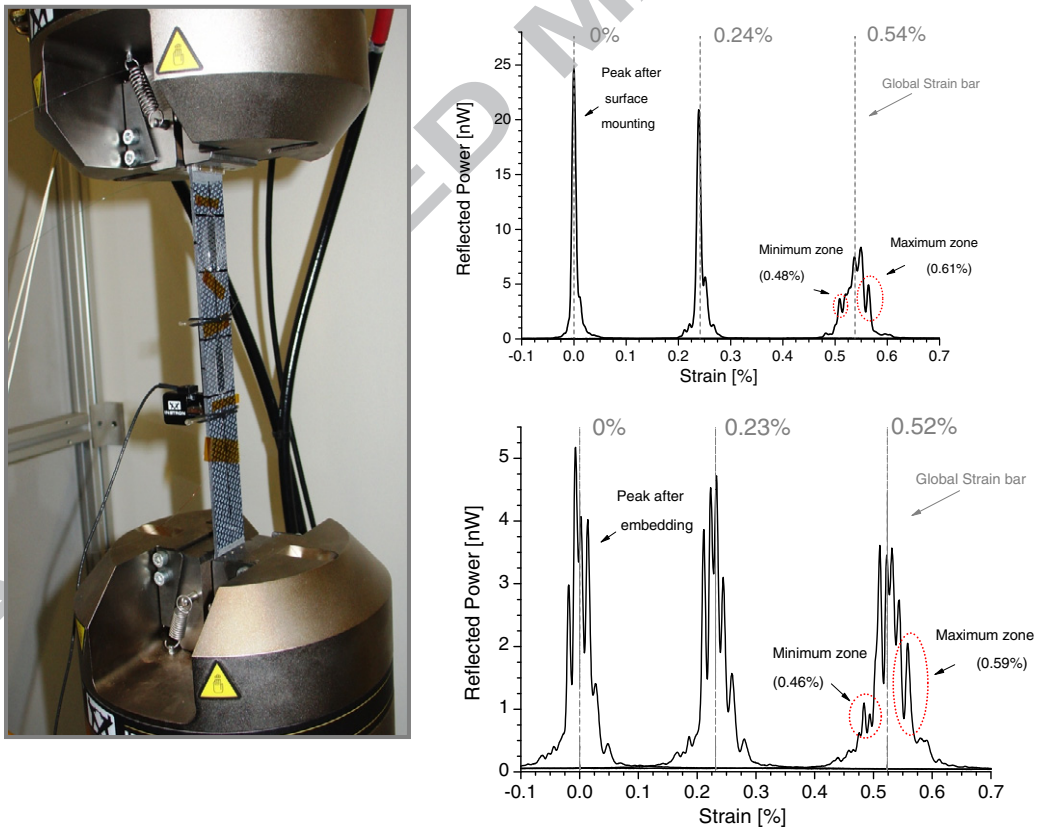

Figure 4. **Tensile test setup, typical deformed spectra of a surface mounted and embedded FBG.**

a)

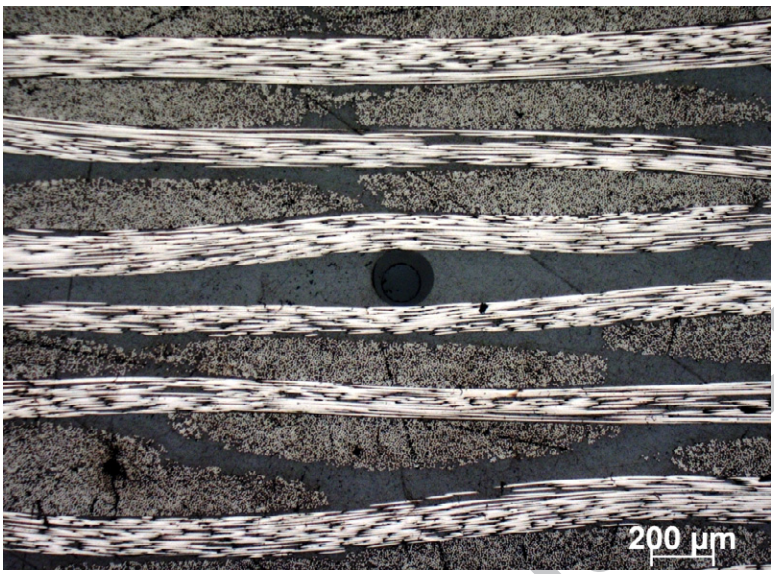

b)

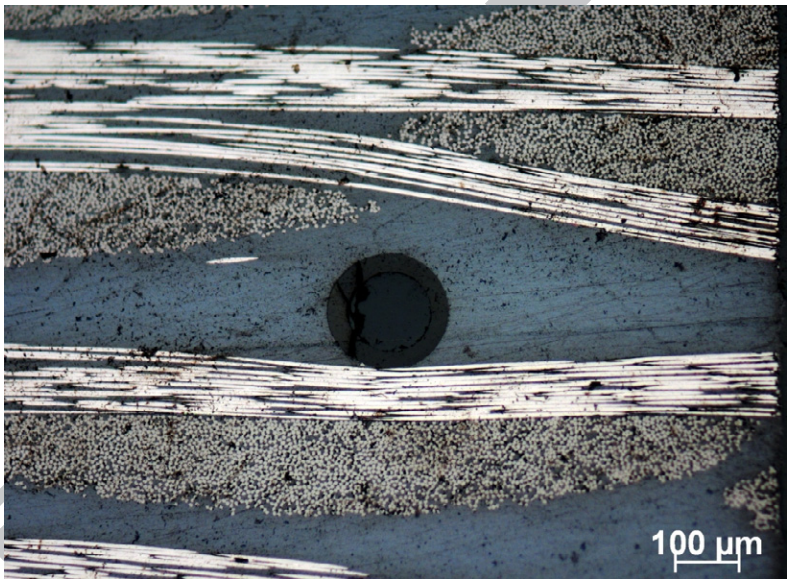

Figure 5. **a, b) Cross-sectional view of composite along the length of the optical fibre.**

a)

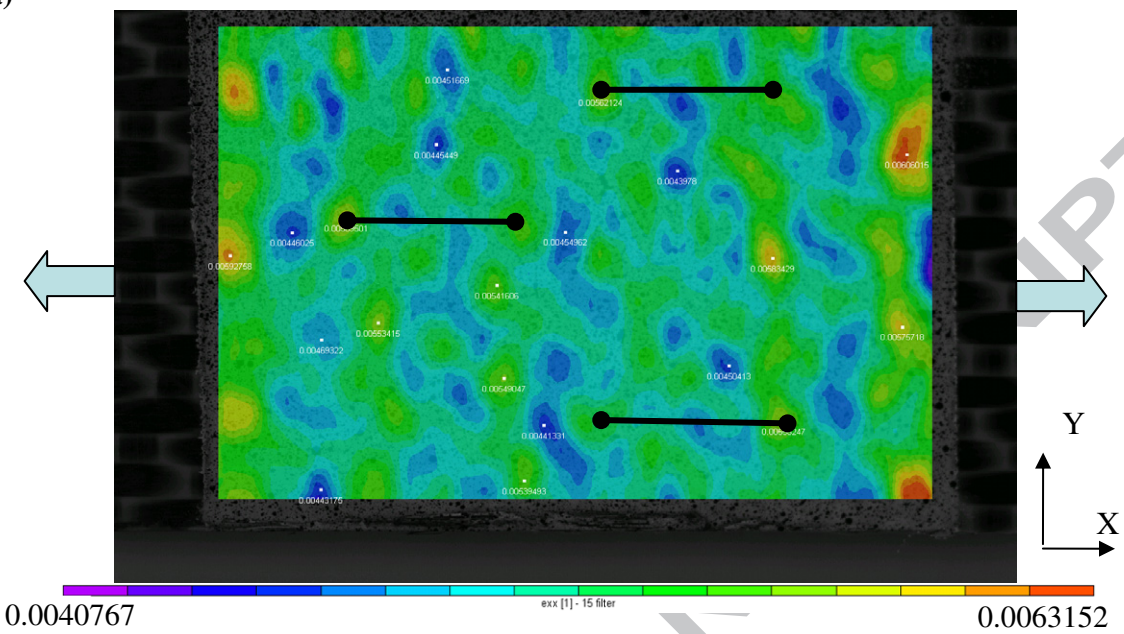

0.0040767 0.0063152

b)

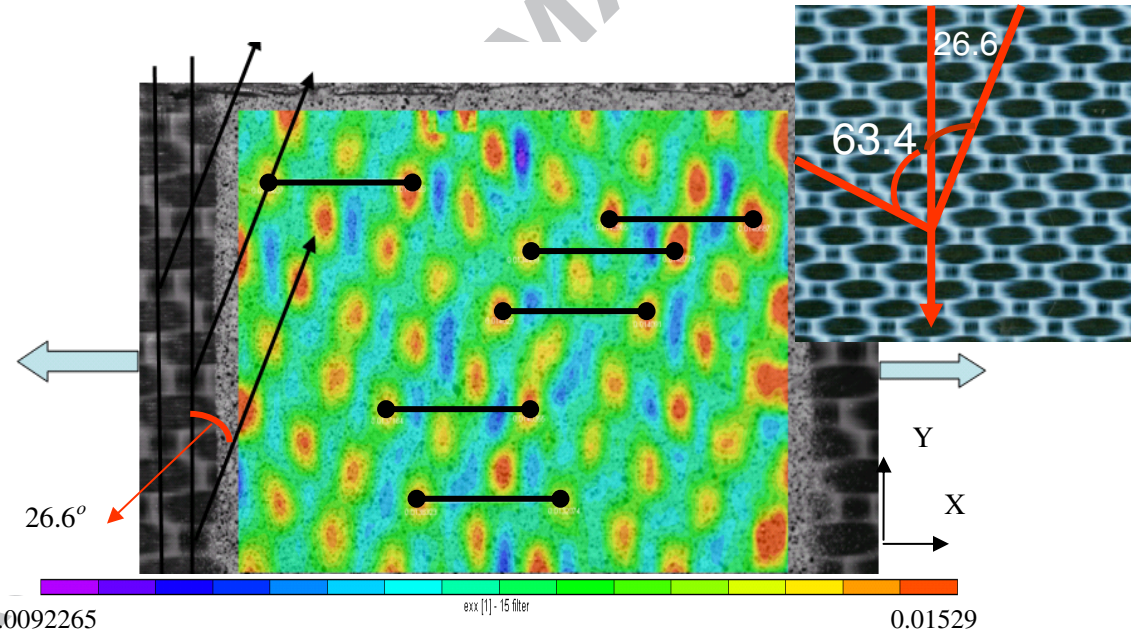

0.0092265 0.01529

c)

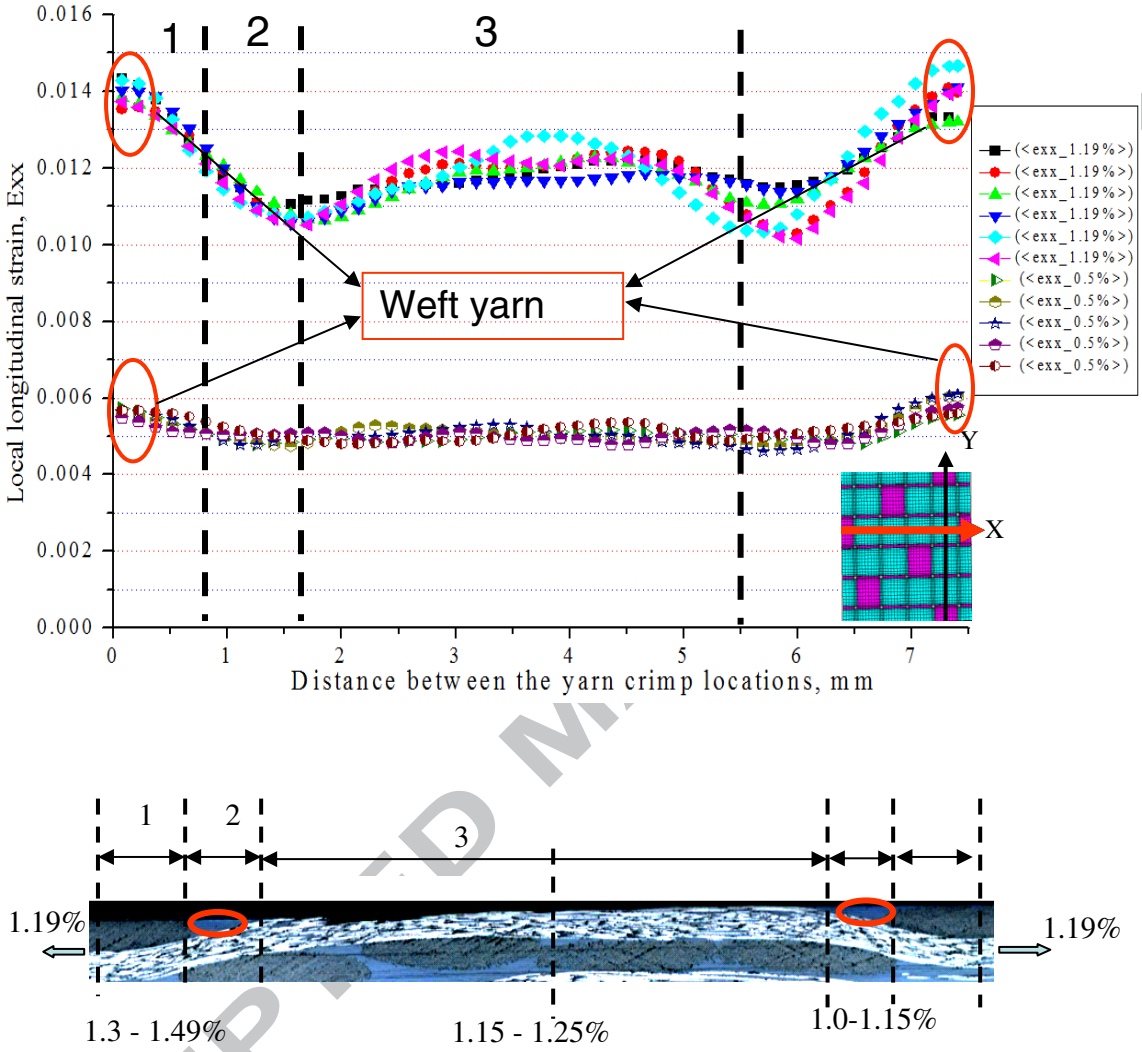

Figure 6. **Local strain analysis: a) longitudinal local strain contours at 0.5%; b) longitudinal local strain contours at 1.19%; c) evolution of the local strain profile from 0.5% to 1.19% and the corresponding locations on the laminate cross section.**

a)

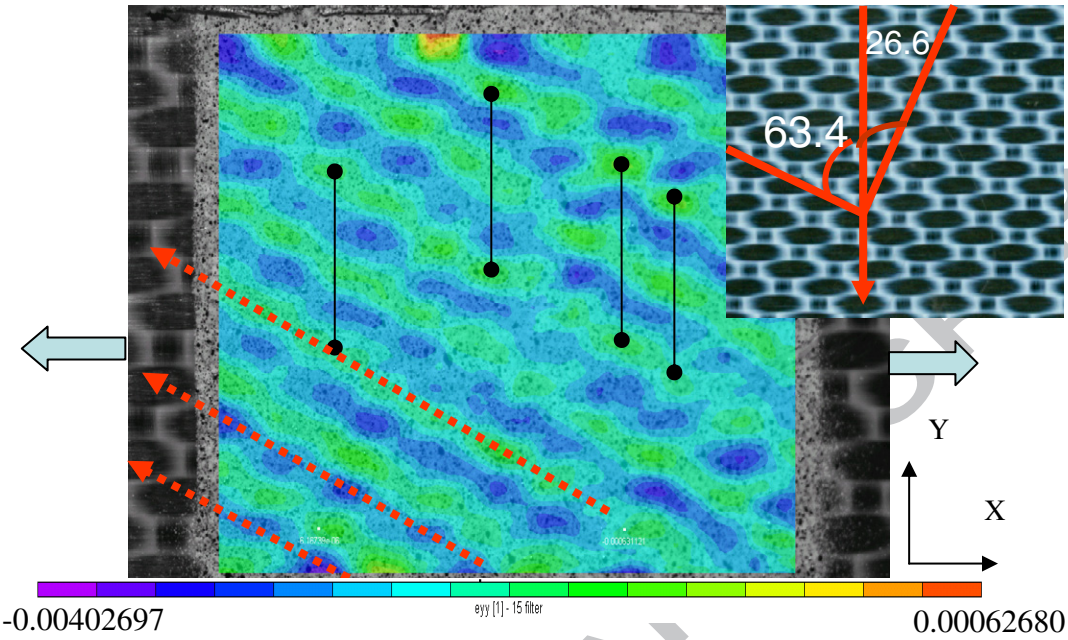

b)

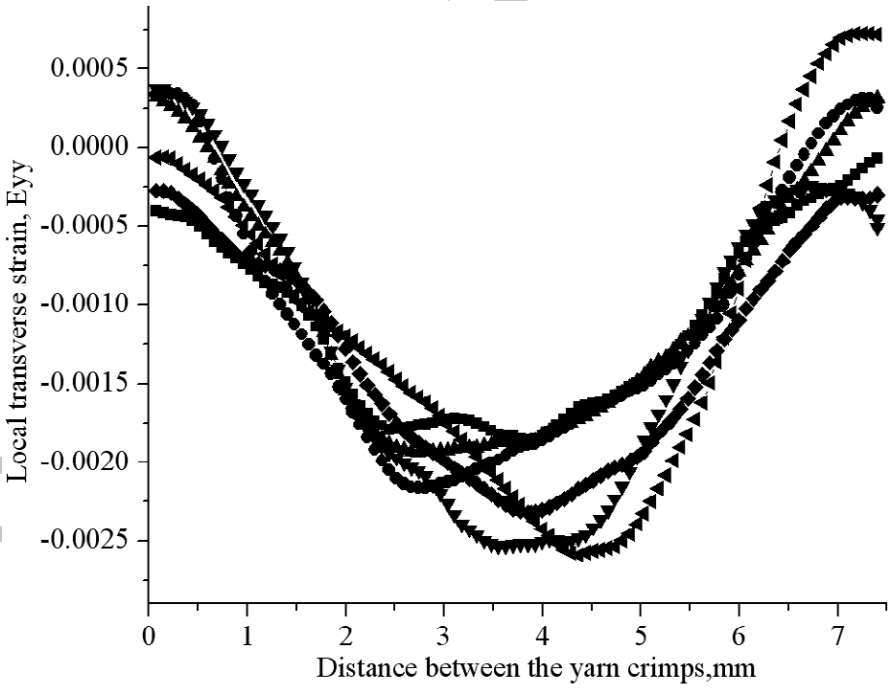

Figure 7. **Transverse strain profiles at 1.19% of average tensile strain: a) ε_{yy} (Contour limits); b) local strain profiles in transverse direction (ε_{yy}).**

a)

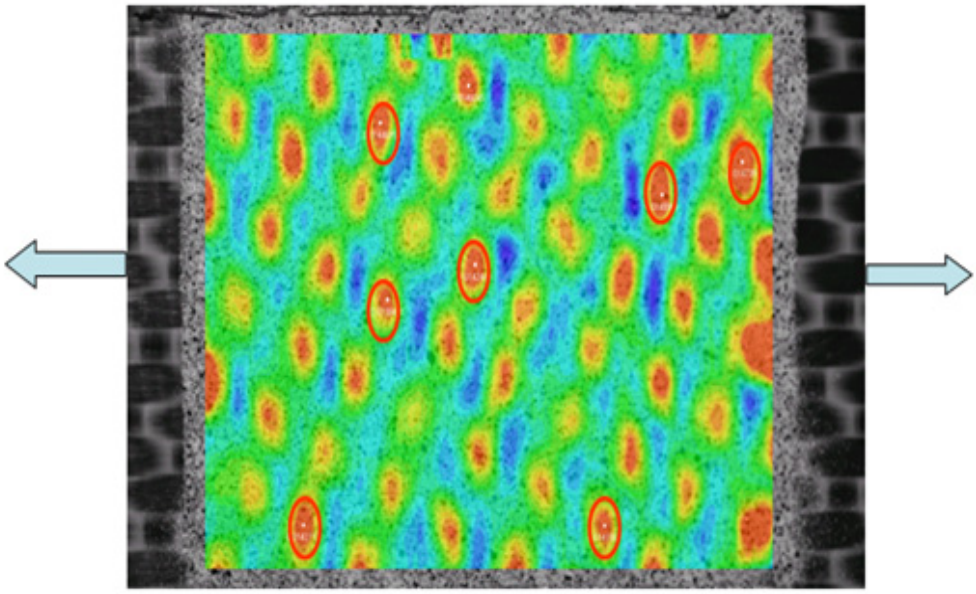

b)

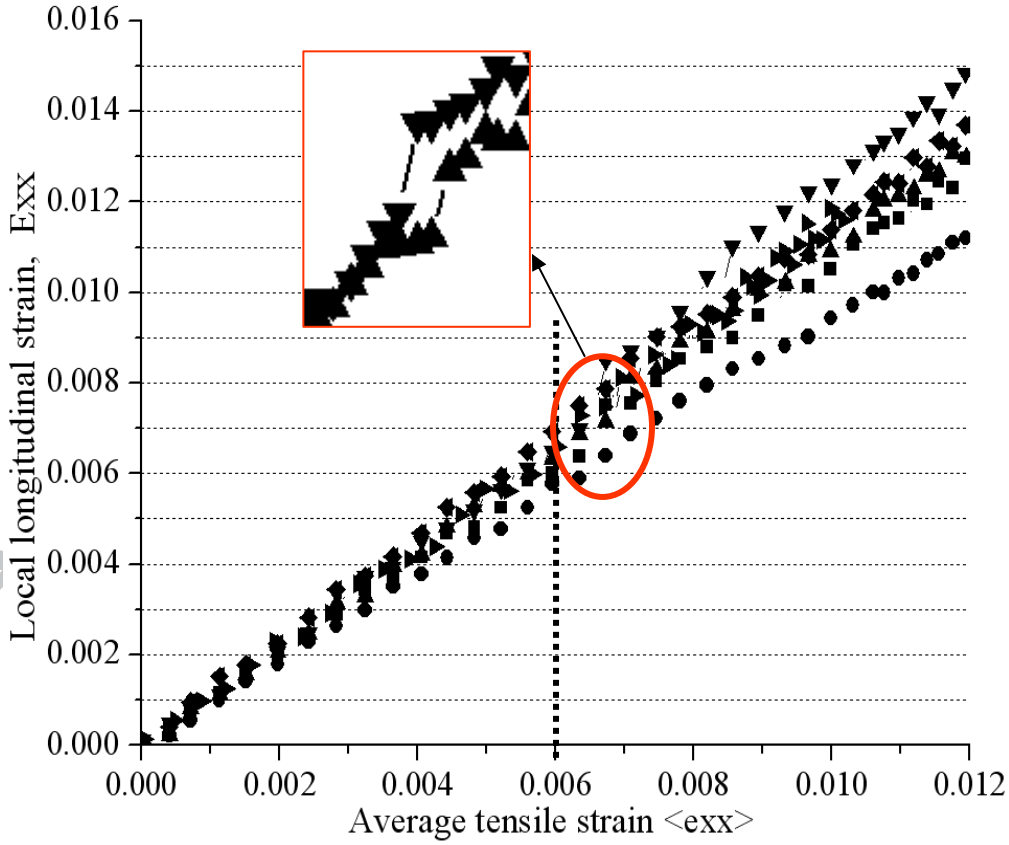

c)

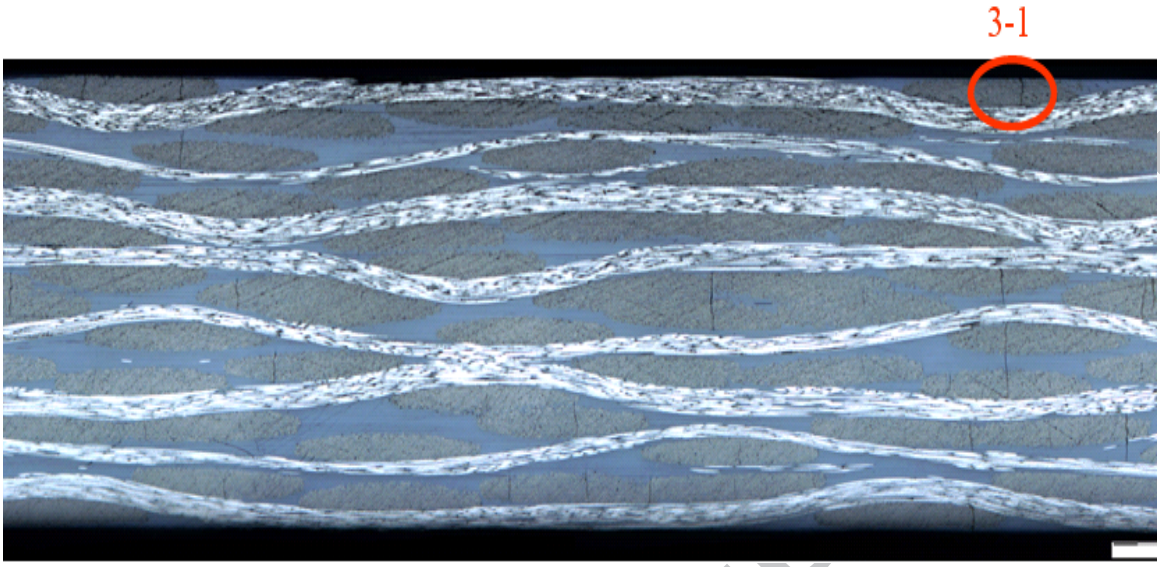

Figure 8. **Damage initiation on the laminate surface: a) non-periodic strain localization on the composite surface; b) local vs. average tensile strain; c) microscopic image of damage initiation on the surface weft yarns at 0.6-0.8% of average tensile strain [27].**